Proposal to search for exotic cascades with CLAS using an untagged virtual photon beam

E. Pasyuk
Arizona State University

R. Schumacher
Carnegie Mellon University

H. Crannell, R. Hakobyan, D. Sober
Catholic University of America

D. Doughty
Christopher Newport University

K. Joo
University of Connecticut

I. Strakovsky
George Washington University

R. DeVita, M. Battaglieri
INFN, Genova

A. Afanasev[‡], S. Boiarinov, W.K. Brooks, V.D. Burkert, P.L. Cole, L. Elouadrhiri, M.M. Ito, B.A. Mecking, M.D. Mestayer, E.S. Smith[*†], S. Stepanyan[*]
Jefferson Lab

V. Batourine, W. Kim, and K. Park
Kyungpook National University, South Korea

P. Bosted[‡]
University of Massachusetts

J. Calarco, M. Holtrop [*]
University of New Hampshire

D.S. Carman, K. Hicks, A. Tkabladze
Ohio University

T. Nakano[‡]
Research Center for Nuclear Physics of Osaka University

[†]Contact person
[‡]Limited Member
[*]Co-spokesperson

V. Kubarovsky
Rensselaer Polytechnic Institute

L. Todor
University of Richmond

R. Gothe*, J. Langheinrich, D.J. Tedeschi, M. Wood
University of South Carolina

and the CLAS Collaboration

Abstract

We propose to use CLAS to measure the production of pentaquark cascade states using a 5.7 GeV electron beam incident on a deuterium target but without detecting the scattered electron. This untagged virtual photon beam is necessary to achieve sufficient sensitivity to the expected small cross sections, but the method requires the direct reconstruction of the cascades using their decay products. The sequence of weakly decaying daughter particles provides a powerful tool to pick out the reactions of interest. Using the available theoretical estimate for the production cross section of 10 nb, we expect to detect 460 Ξ_5^{--} particles during a 20 day run. Together with our estimate for the background levels, this represents a statistically significant result.

CVS: docs/clas_analysis/cascades
Original: December 5, 2003

Contents

1 Introduction

In the past year there have been six experimental observations [1, 2, 3, 4, 5, 6, 7] of a narrow exotic S=+1 baryon state at a mass of approximately 1.54 GeV. These observations appear to confirm the existence of the Θ^+, which is the predicted spin 1/2, isospin 0, member of the anti-decuplet of baryons within the Chiral Soliton Model [8]. The anti-decuplet (see Fig. 1) contains three explicitly exotic states whose quantum numbers require a minimal quark content of 4 quarks and 1 anti-quark. These exotic states cannot be accommodated within the simple quark model which assumes all baryons are built out of 3 quarks. Besides the Θ^+, the other exotic states have S=-2 and charge Q=-2 and Q=+1, which we will denote by Ξ_5^{--} and Ξ_5^+ respectively. The subscript "5" indicates the five-quark (pentaquark) nature of the states and is used to distinguish them from ordinary cascade states. These exotic cascade states have isospin 3/2. Two additional partners, denoted Ξ_5^- and Ξ_5^0, are also 5-quark states but are not explicitly exotic.

The NA49 collaboration has recently reported evidence for the Ξ_5^{--} and the Ξ_5^0 at a mass of 1.86 GeV [10]. The states were reconstructed from their decay products using their decays into $\Xi_5^{--} \to \Xi^-\pi^-$ and $\Xi_5^0 \to \Xi^-\pi^+$. These observations are critical for verifying the existence of the anti-decuplet of pentaquarks, and require confirmation. We note, for example, that the WA89 experiment [11] with a much larger statistical sample has not been able to confirm this observation yet. Finally, the third exotic state, Ξ_5^+, must be found at a mass close to the measured value of 1.86 GeV of the Ξ_5^{--}. Establishing the existence of the Ξ_5^- and the Ξ_5^0 states with similar widths and masses will also be a strong confirmation of the anti-decuplet structure of particles.

The purpose of this proposal is to search specifically for the Ξ_5^{--}, Ξ_5^- and the Ξ_5^0 of the anti-decuplet with the CLAS detector. The search will also include the Ξ_5^+, but with reduced sensitivity. This paper will review the possible reactions which can be used for such a search, and then conclude that the best option for detecting these states is to use a high intensity untagged virtual photon beam incident on a deuterium target.

2 Experimental overview

The major experimental problem in detecting the cascade pentaquark states is the expected low rate of events. The low photoproduction cross sections (expected to be about 10 nb) and small phase space (two K mesons must be produced in association with the 1.8 GeV state) translate into a small production rate. For this reason, we need the highest possible value of luminosity. In order to maximize the production cross-section, we must run at very small values of Q^2. Small Q^2 and high luminosity

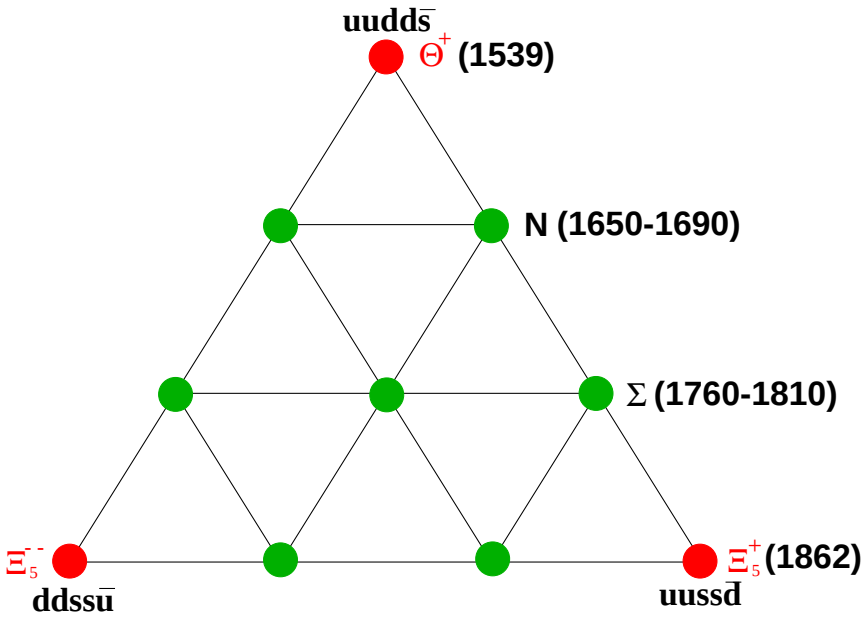

Figure 1: Anti-decuplet predicted by the chiral soliton model [9]. The masses in parenthesis are updated values for the predicted masses. The red corners of the anti-decuplet have exotic quantum numbers. The quark content of the exotic members are also displayed.

means that we must use either an untagged photon beam produced at the tagger, or an untagged electron beam (i.e. run the electron beam through the CLAS target, but don't require an explicit electron trigger, thus effectively triggering on very low-angle and hence, low Q^2, scattered electrons).

The use of untagged beams means that we can no longer use a missing mass technique to detect the two kaons and look for the recoil mass of the cascade. Instead we directly detect the decay products and form the invariant mass. This alternative technique does have some advantages. First, the daughter decay products (Ξ^-, Σ, and Λ) decay weakly with decay distances of several centimeters. The CLAS vertex resolution is on the order of several millimeters giving good efficiency for this detached vertex technique. This technique is particularly good at rejecting the combinatorial background from non-strange, large multiplicity events. Secondly, the direct detection technique is sensitive to the semi-inclusive cross-section for cascade production; we don't lose the events if one or more of the kaons is actually a vector K*.

We give details in later sections, but to summarize: we plan to run an "untagged" electron beam on a deuterium target at the maximum luminosity compatible with drift chamber operation ($\sim 10^{34} cm^{-2} s^{-1}$) and to cut down the large and uninteresting

low-multiplicity hadronic event rate by a restrictive trigger demanding charged tracks in at least 3 of the 6 sectors of CLAS.

3 Production and decay modes

In Table 1 we list the exclusive production modes of exotic cascades off a proton target. All Ξ_5 particles can be produced, but with different production thresholds corresponding to the associated production of only two kaons (threshold = 3.9 GeV) or two kaons and a pion (threshold = 4.3 GeV). The identification of the Ξ_5^{--} and the Ξ_5^{+} in missing mass require the detection of either three or four particles to determine the mass of the undetected cascade.

In Table 2 we list the production modes for exotic cascades off a neutron target. In this case, nuclear targets must be used, and the missing mass technique is limited by the Fermi motion in the target. Therefore, it is necessary to reconstruct the cascade particles from their decay products.

As explained in the overview we will not use the missing mass technique but will rely on the direct detection of the decay products of the exotic cascades. The possible decay sequence and products of the Ξ_5 particles are given in Table 3. Indicated in the table are the intermediate narrow particles which can be used to tag the decay sequence, as well as the neutral particles which are the result of the decay. One would like to have decay sequences that result in a few particles all of which are charged. The Ξ_5^{--} has an all-charged decay mode, requiring the detection of three negative pions and one proton. The Ξ_5^{+} has only one all-charged decay mode, but requires the detection of two negative and three positive particles. A more practical decay mode is the one that results in the production of three pions and one neutron. A similar decay mode results from the decay of the Ξ_5^{-}. The Ξ_5^{0} has a decay mode that results in three pions and one proton. Throughout we have considered only the charged $p\pi^-$ decay mode of the Λ. In principle, all four Ξ_5 particles are accessible to CLAS, but the observations of the Ξ_5^{--} and the Ξ_5^{0} are the most promising. The Ξ_5^{-} and the Ξ_5^{+} require the detection of a neutron in the final state.

4 Factors affecting signal extraction

We review various factors which affect the experimental determination of cascade production.

Table 1: Production of Ξ_5 off a proton target. The first column gives the reaction channel, the second column lists the particles which must be detected if the state is identified by missing mass, the third column gives the energy threshold for the reaction, the fourth column shows the mass constraints which can be brought to bear on this case, and the fifth column provides estimates for the cross section. Except where referenced, all cross sections are rough estimates.

Reaction	Particles Detected in Missing Mass Mode	Threshold (GeV)	Mass Constraints	σ (nb) (Estimate)
$\gamma p \to K^+K^+\pi^+\Xi_5^{--}$	$K^+K^+\pi^+$	4.3		1
$\gamma p \to K^+K^+\Xi_5^-$	K^+K^+	3.9		10
$\gamma p \to K^+K^0\Xi_5^0$	$K^+(\pi^+\pi^-)$	3.9	K^0	5
$\gamma p \to K^0K^0\Xi_5^+$	$(\pi^+\pi^-)(\pi^+\pi^-)$	3.9	2 K^0	1 [12]
$\gamma p \to K^+K^0\pi^-\Xi_5^+$	$K^+(\pi^+\pi^-)\pi^-$	4.3	K^0	0.1

4.1 Production cross section

There is only one calculation of the production cross section of exotic cascades with photon beams [12] which is illustrated in Figs. 2 and 3. The calculations are for $\sigma(\gamma n \to K^+K^+\Xi^{--})$ and for $\sigma(\gamma p \to K^0K^0\Xi^+)$, corresponding to similar reaction channels for the neutron and proton. The predictions off a neutron target are generally about an order-of-magnitude larger than off the proton (see Tables 1 and 2). The dominant mechanism for production off the neutron is charged K^+ exchange, so uncertainties in the $g_{K^*N\Xi}$ coupling constant do not change the predictions very much. Conversely, the production off the proton varies by orders of magnitude depending on the value of the $g_{K^*N\Xi}$ coupling. For the best-guess value of $g_{K^*N\Xi}$=-1.8, production off the proton is 10 times smaller than the production off the neutron. At $E_\gamma = 5$ GeV, $\sigma(\gamma n \to K^+K^+\Xi^{--}) \sim 10$ nb and $\sigma(\gamma p \to K^0K^0\Xi^+) \sim 1$ nb. [1]

There are no other calculations of the cross section. But we can attempt to estimate the production cross sections by scaling the above calculations by assuming that the same production mechanism dominates. In this way we have obtained the values shown in Table 1 and 2. These are meant as rough guides as to what one might expect, but should be replaced with actual calculations when they become available.

[1]The calculations assume positive parity for the Ξ_5 states, which is consistent with the chiral soliton model. Negative parity states would have smaller cross sections.

Table 2: Production of Ξ_5 cascades off a neutron target. The Ξ_5 particles must be reconstructed using the particles from their decay. Except where referenced, all cross sections are rough estimates.

Reaction	Threshold	σ (nb) (Estimate)
$\gamma n \to K^+K^+\Xi_5^{--}$	3.9	10 [12]
$\gamma n \to K^+K^0\Xi_5^{-}$	3.9	5
$\gamma n \to K^0K^0\Xi_5^{0}$	3.9	1
$\gamma n \to K^0K^0\pi^-\Xi_5^{+}$	4.3	0.1

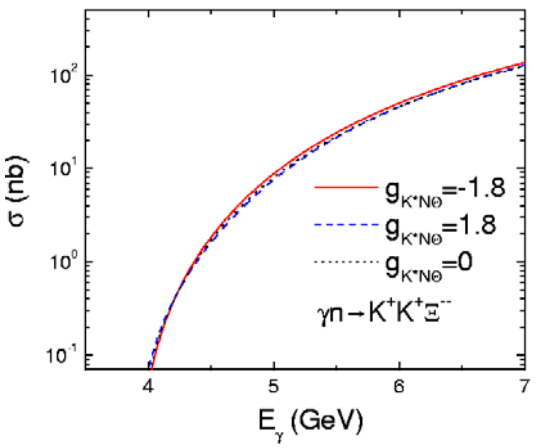

Figure 2: Cross section for the production of $\gamma n \to K^+K^+\Xi^{--}$ [12].

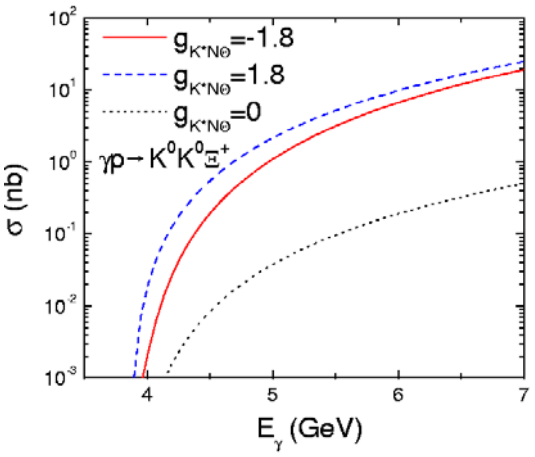

Figure 3: Cross section for the production of $\gamma p \to K^0K^0\Xi^{+}$ [12].

4.1.1 Threshold

The effect of threshold of the reaction can be estimated based on phase space production. At 5 GeV we estimate that the production of reactions with a threshold of 4.3 GeV will be suppressed by 30% relative to reactions with a threshold of 3.9 GeV. This is the penalty paid, in addition to any loss of acceptance, for creating an additional pion in the final state (Tables 1 and 2).

Table 3: Decay sequences for the Ξ_5 cascade particles. The first three columns give the decay sequence, and the decay products are grouped by parentheses. The numbers in parentheses in the first column give the branching fraction to this mode ignoring phase space factors [14, 15, 9]. The last three columns give the mass constraints which can be brought to bear in this reaction, the neutral particles among the decay products, and the overall branching fraction to this decay mode. We note that we give only the most promising modes for detection with CLAS; other modes can also be reconstructed with lower efficiency. The branching fraction for $\Lambda \to p\pi^-$ is 0.64, and the branching fraction for $\Sigma^+ \to n\pi^+$ is 0.48. The probability of the $\overline{K}^0$ to decay via $K_s \to \pi^+\pi^-$ is 0.34. The other decay branches are close to 100%.

Primary decay	Secondary decay	Tertiary decay	Mass Constr.	Q=0	Br.
$\Xi_5^{--} \to \pi^-\Xi^-$ (0.5)	$\to \pi^-(\pi^-\Lambda)$	$\to \pi^-\pi^-(\pi^-p)$	Ξ^-, Λ		0.32
$\Xi_5^{--} \to K^-\Sigma^-$ (0.5)	$\to K^-(\pi^-n)$		Σ^-	n	0.5
$\Xi_5^- \to \pi^0\Xi^-$ (0.33)	$\to \pi^0(\pi^-\Lambda)$	$\to \pi^0\pi^-(\pi^-p)$	Ξ^-, Λ	π^0	0.21
$\Xi_5^- \to \pi^-\Xi^0$ (0.17)	$\to \pi^-(\pi^0\Lambda)$	$\to \pi^-\pi^0(\pi^-p)$	Ξ^0, Λ	π^0	0.11
$\Xi_5^- \to \overline{K}^0\Sigma^-$ (0.17)	$\to (\pi^-\pi^+)(\pi^-n)$		K_s, Σ^-	n	0.06
$\Xi_5^- \to K^-\Sigma^0$ (0.33)	$\to K^-(\gamma\Lambda)$	$\to K^-\gamma(\pi^-p)$	Σ^0, Λ	γ	0.21
$\Xi_5^0 \to \pi^0\Xi^0$ (0.33)	$\to \pi^0(\pi^0\Lambda)$	$\to \pi^0\pi^0(\pi^-p)$	Ξ^0, Λ	2 π^0	0.21
$\Xi_5^0 \to \pi^+\Xi^-$ (0.17)	$\to \pi^+(\pi^-\Lambda)$	$\to \pi^+\pi^-(\pi^-p)$	Ξ^0, Λ		0.11
$\Xi_5^0 \to K^-\Sigma^+$ (0.17)	$\to K^-(\pi^+n)$		Σ^+	n	0.09
$\Xi_5^0 \to \overline{K}^0\Sigma^0$ (0.33)	$\to (\pi^+\pi^-)(\gamma\Lambda)$	$\to \pi^+\pi^-\gamma(\pi^-p)$	K_s, Σ^0, Λ	γ	0.07
$\Xi_5^+ \to \pi^+\Xi^0$ (0.5)	$\to \pi^+(\pi^0\Lambda)$	$\to \pi^+\pi^0(\pi^-p)$	Ξ^0,Λ	π^0	0.32
$\Xi_5^+ \to \pi^+\pi^+\Xi^-$ (?)	$\to \pi^+\pi^+(\pi^-\Lambda)$	$\to \pi^+\pi^+\pi^-(\pi^-p)$	Ξ^0,Λ		?
$\Xi_5^+ \to \overline{K}^0\Sigma^+$ (0.5)	$\to (\pi^+\pi^-)(\pi^+n)$		K_s, Σ^+	n	0.09

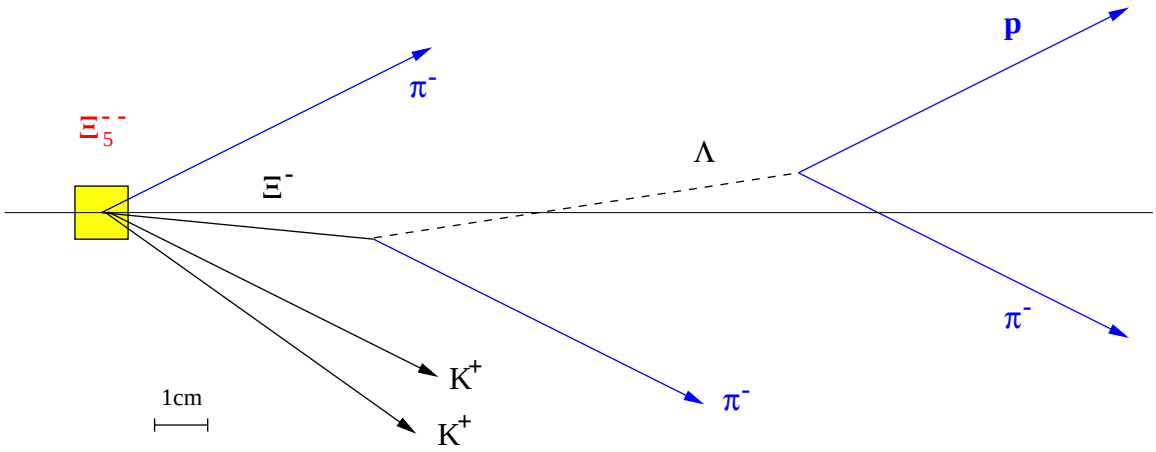

Figure 4: A graphical display of typical distances in the associated production of $\gamma n \to K^+K^+\Xi_5^{--}$ and decay for the Ξ_5^{--}. The particles that decay weakly have vertices displaced by the decay distance $c\tau$. The average value of $\gamma\beta$ is approximately 1.3 as shown in Fig. 5. This experiment will require the detection of the particles in blue (three negative pions and the proton). The kaons could be used as additional tags, but are currently assumed to go undetected.

4.2 Branching fraction

A specific final state is reached via several decays as given in Table 3. The number of events which result in that particular topology is proportional to the product of branching ratios in the decay sequence. These are given in the last column of the table. The sum of the branching fractions for each particle typically adds up to only 50% because only the most promising branches are included. Other decay modes, such as $\Lambda \to n\pi^0$, will have a small reconstruction efficiency in CLAS. For example, the total branching fraction $\Xi_5^{--} \to \pi^-\pi^-\pi^-p$ is 32%, and the branching fraction $\Xi_5^{+} \to \pi^+\pi^-\pi^+n$ is 9%.

4.3 Signal-to-background

The ease of extraction of the signal for cascade production depends on both the rate of production of the signal as well as the amount of background, both physical as well as instrumental. The determination of the cascade signal using missing mass techniques is limited by misidentification and combinatorial backgrounds of the associated particles. In the experiment with the highest rate of tagged photons (g6c), the main source of backgrounds comes from misidentifying pions as kaons. In this case the signal-to-background for excited cascade production is approximately 0.1. The back-

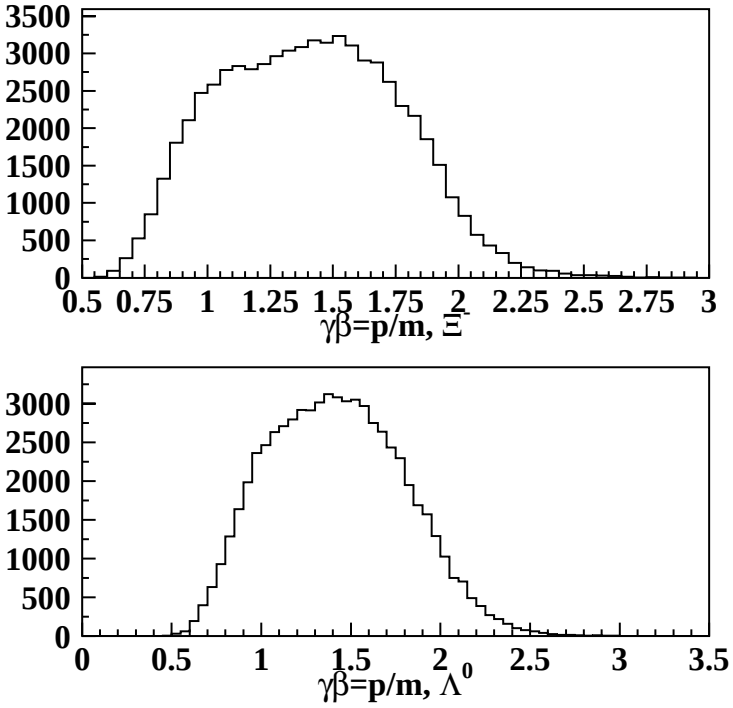

Figure 5: Values of $\gamma\beta$ for the Ξ^- (top) and Λ (bottom) from the decay sequence of the Ξ_5^{--}.

ground situation can be improved at lower photon fluxes because these backgrounds are proportional to the square of the flux, but requires longer running periods.

The decay sequence of the Ξ_5^{--} (Fig. 4) provides the answer on how to cleanly identify these particles. The primary decay products of the Ξ_5 particles decay weakly and therefore result in detached vertices several centimeters downstream of the primary interaction. Often there is also a second weak decay with a second detached vertex even further away. The decay lengths of the particles will be stretched by the kinematic factors ($\gamma\beta$) of the reaction (see Section 8), which are plotted in Fig. 5. The average value is approximately 1.5. If one reconstructs the final state particles, the detached vertices reconstructing to narrow particles can be used to identify the exotic cascades. We note that the vertex resolution of CLAS for reconstructing electrons is approximately 0.2 cm (Fig. 6) [13]. However, reconstructing detached vertices increases the uncertainty. The resolution in the azimuthal (ϕ) direction is 4-6 times

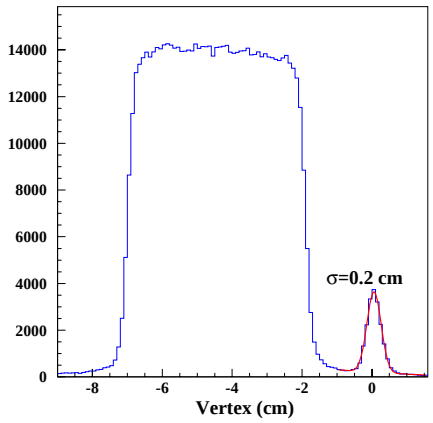

Figure 6: Reconstructed z-vertex resolution for electrons in a 5.7-GeV inbending electron beam. The peak at the origin is due to a thin window downstream of the target.

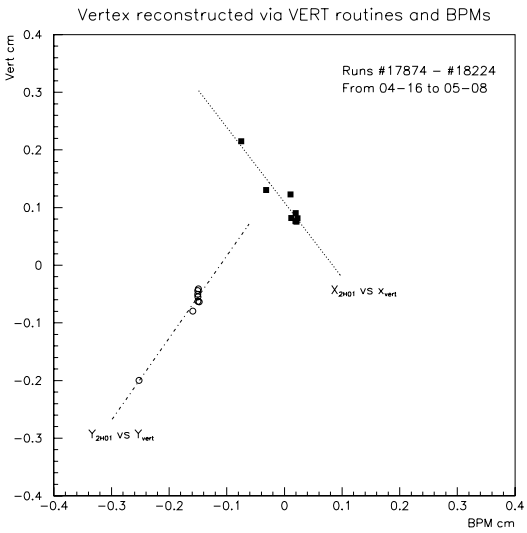

Figure 7: Beam position as reconstructed using multi-track events vs. the beam position as determined by the beamline BPMs. The open circles are for the vertical position and the filled squares measure the horizontal position.

more than in the bend plane (θ). The combination of these resolution functions require that, in order not to loose significant efficiency for detection of Λs, the selection of proton and pion daughter particles using the distance of closest approach of the two tracks needs to be fairly loose, on the order of about 2 cm. However, the systematic uncertainties in vertex reconstruction are very small. In Fig. 7 we show that the average beam position as determined by multi-track vertex reconstruction is consistent with the measurements by the beam position monitors (BPMs). The beam position using multi-track events was averaged over the period of a run and agrees to the position given by the BPMs to fractions of a mm over the course of three weeks.

4.4 Choice of target

There are several choices for neutron targets. The simplest nucleus is deuterium which minimizes any nuclear effects, if present. The only small disadvantage to this target is that there is a limit to how thin one can make a practical target (~ 0.5 cm). However, due to the expected uncertainty in vertex reconstruction, we do not expect that the target length will add significantly to the uncertainty in vertex reconstruction. Also,

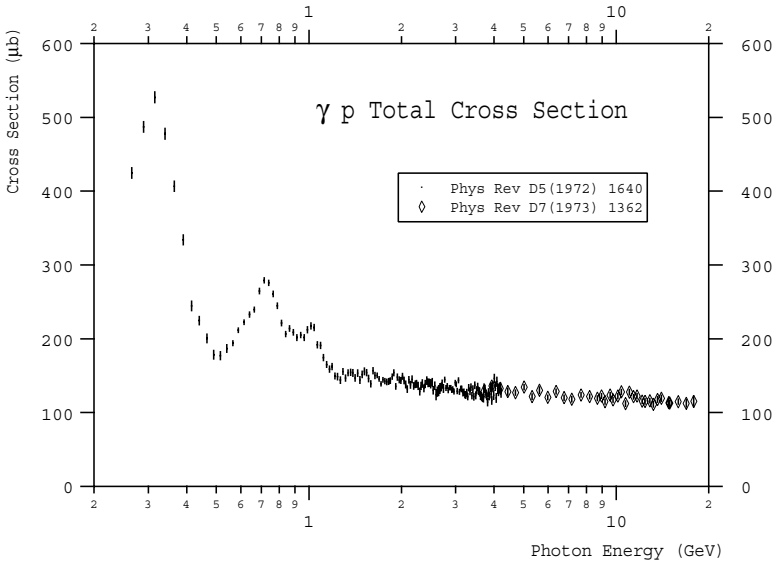

Figure 8: Total photoproduction cross section on the proton as a function of the photon beam energy.

if we use 12 μm Al foils for the target windows, they would constitute only 9% of the target thickness. We note that the precise target thickness is not needed for this application, and the walls can also serve as valid neutron targets, so any difficulties in controlling the target length during manufacturing are relaxed. Therefore, our present choice is to use a short deuterium target cell. [2]

5 Luminosity and rate estimates

The total cross section for photoproduction $\sigma_{\gamma p}$ is shown in Fig. 8. The estimated hadronic rates are obtained by integrating the photon flux, either virtual or real, over the total cross section. In Appendix A we review and compare the untagged photon fluxes produced using a radiator upstream of the tagger spectrometer and the virtual photon flux in the target produced by an untagged electron beam. Although there are advantages and disadvantages to each method, the maximum flux is obtained with an untagged electron beam, which we use below to estimate our production rates.

The untagged virtual photon flux from an electron beam can be approximated

[2]If an untagged real photon beam is used –not presently favored– then thin ^7Li targets would be considered.

with the following formula:

$$\Gamma = \frac{\alpha}{\pi}\frac{1}{E-E'}\left(1+(1-w)^2\right)\ln\left(\frac{\theta_{max}}{\theta_{min}}\right), \quad (1)$$

$$\theta_{min} = \frac{m_e}{E} \quad (2)$$

$$\theta_{max} = 0.175 \quad (3)$$

$$w = 1-\frac{E'}{E} \quad (4)$$

$$\Gamma = 3.7\times10^{-3} \quad (5)$$

where E and E' are the energy of the incident and scattered electrons respectively, and θ_{max} and θ_{min} correspond to the minimum and maximum angles of the scattered electron. The virtual photon flux Γ has been integrated and cut off below the critical angle. The rate of reconstructed cascades is given by

$$Rate(Hz) = \Gamma\times L\times\Delta E\times\sigma_\Xi\times Br\times Acc, \quad (6)$$

$$L = 10\,nb^{-1}s^{-1} = 10^{34}cm^{-2}s^{-1} \quad (7)$$

$$\Delta E = 1.5GeV \quad (8)$$

$$\sigma_\Xi = 10\,nb, \quad (9)$$

$$Br(\Xi_5^{--}\to\pi^-\pi^-\pi^-p) = 0.32 \quad (10)$$

$$Acc = 1.5\times10^{-3} \quad (11)$$

The rate at this luminosity is approximately 0.00027 Hz, or a total of 460 cascades produced and reconstructed during a 20 day run.

5.1 Trigger

The total cross section for photoproduction $\sigma_{\gamma p}$ is shown in Fig. 8. At a luminosity of $L = 10^{34}cm^{-2}s^{-1}$, the inelastic rate for hadron production is 220 kHz for a 5.7 GeV beam. The rates are dominated by the cross section for single pion production, which peaks at 0.3 GeV, which is exacerbated by the $1/E_\gamma$ dependence of the photon flux. The inclusive hadron production for photon energies below 4 GeV is 213 KHz. In the energy region of interest to this proposal, the cross section is dominated by multi-pion production. In order to run at the highest luminosity, a trigger scheme must be developed which reduces the rates to a level which can be accommodated by the present DAQ system.

The event size has been parametrized for various electron run periods as follows:

$$\text{Event Size (kB)} = c_1 + c_2\times L, \quad (12)$$

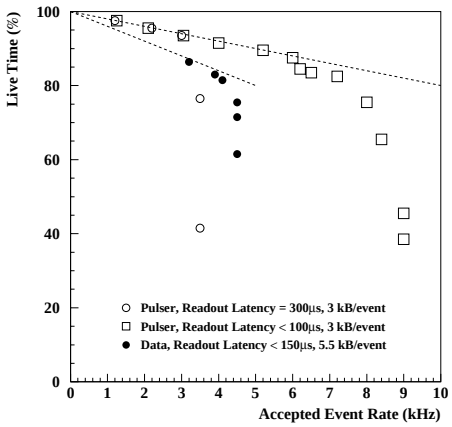

Figure 9: Live time as a function of event rate for the CLAS detector showing typical maximum event rates. The solid circles show the capabilities of current operation.

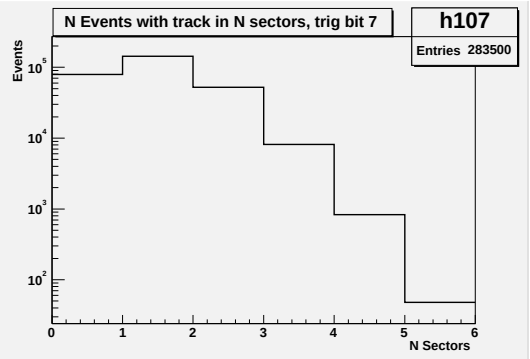

Figure 10: Number of "unbiased" events from the e6 data period as a function of the number of sectors with tracks. The fraction of events with tracks in 3 or more sectors is 4% of the total. The e6 data was run under conditions similar to those expected for this run.

where L is the luminosity in units of 10^{34}cm^{-2}s^{-1}, and c_1 and c_2 are constants which depend on the trigger energy thresholds and B-field settings. For e1-6 (H2, 5.7 GeV), c_1=2.4 and c_1=3, for e1c (H2, 4.2 GeV), c_1=3.8 and c_1=3, and for e6 (D2, 5.7 GeV), c_1=2.4 and c_1=1.5 The experimental conditions of e6 are very similar to our proposal (beam energy=5.7 GeV, reversed field at 2250 A), so we expect an event size of approximately 4 kB.

In Fig. 9 we plot the live time of the DAQ system as a function of the accepted trigger rate. It indicates that the present system is limited to a trigger rate of approximately 4 KHz. Increasing this limit to 10 kHz is possible with the addition of additional computing power in the front-end processors. The front-end CPU's are presently being upgraded and it is expected that the rate limit will be increased to 10 kHz by mid 2004. Nevertheless, the dead time due to the conversion in the front-end modules will increase linearly to approximately 40% at the 10 kHz rate. See Appendix B for additional details.

Many events which are written to tape during an electron run were triggered on hadrons, and the electron is lost down the beampipe. [3] Using this "unbiased"

[3]We note that approximately 80% of triggers taken during high-energy electron running do not have an electron, and serve as a sample of "unbiased" events for untagged data.

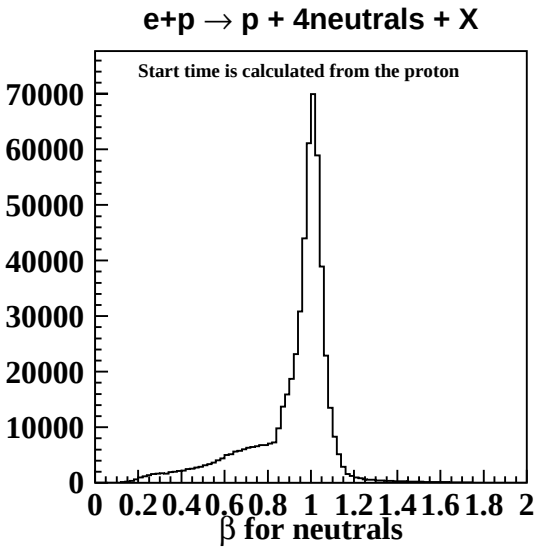

Figure 11: Distribution of calculated velocities of neutral hits in the calorimeter relative to the proton vertex time in the event. A clear peak is found for identified photons.

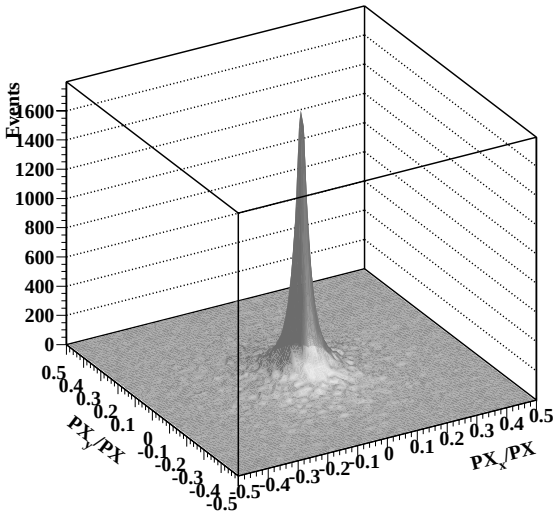

Figure 12: Fraction of y-component of missing momentum vs. x-component of missing momentum, showing that these events indeed are missing an electron scattered practically at zero degrees.

data sample from the e6 running period, we can estimate the trigger rate when we require tracks in three different sectors and also require a minimum-ionizing hit in one calorimeter. The number of "unbiased" events is plotted in Fig. 10 as a function of the number of sectors with tracks. If we require at least three sectors, the number of events satisfying this requirement is only 4% of the total. From this we estimate that the total hadronic rate accepted by both Level 1 and Level 2 triggers will be 220 KHz x 0.04 = 8.8 KHz.

6 Reconstruction of untagged real photon data

In this section we discuss the reconstruction of untagged and multi-particle events. The standard algorithms in CLAS data analysis rely on obtaining accurate timing information from the electron: the scattered electron in electron running and the tagged electron in photon running. For the present proposal for using an untagged beam, we will have neither as a starting point. Here we give proof-of-principle examples of reconstructing data without making use of the scattered electron and demonstrate that

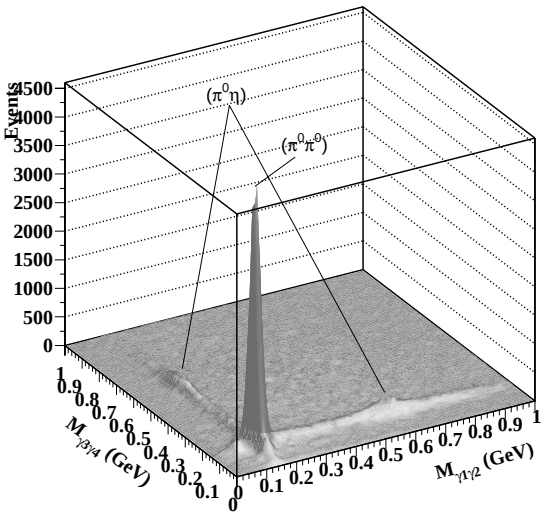

Figure 13: Reconstructed π^0 and η mesons using photons in the calorimeter. The timing of the photons are consistent with the timing derived from the proton in the event.

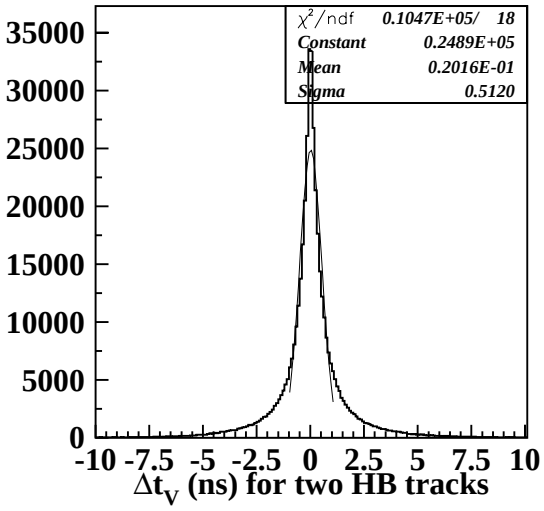

Figure 14: The time difference of two charged tracks reconstructed using their hit positions only. The reconstructed time is quite adequate for use as an input to time-based tracking.

reconstruction of the events in this case can be handled with alternative algorithms.

One practical impact of not detecting the scattered electron is the lack of a precise interaction time for the event. This has a small effect on particle identification, but has almost no effect on tracking. For reactions that have a single charged hadron in the final state, the interaction time can be determined by considering a specific final state. Where multiple tracks are present, the reconstruction can rely on the self-consistency of information from all tracks involved.

6.1 Single charged track events

As an example of reconstructing untagged data, we show the reconstruction of the final state $p\gamma\gamma\gamma\gamma$ from an electron beam run (e1-6). For such untagged events the trigger was produced by an accidental coincidence of an energy deposition in the calorimeter and a signal in the Cerenkov Counter. In the reconstruction the interaction time is calculated assuming that the positive track is a proton. The time-of-flight is then calculated using the measured momentum using hit-based tracking and the exact proton mass. The quality of particle identification for such a reconstruction

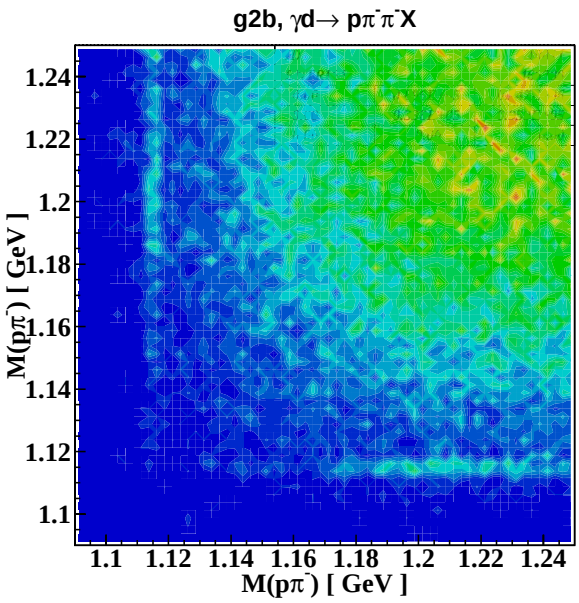

Figure 15: Reconstructed Λ's from the g2b data period. The two combinations of proton and π^- are shown on the two axes and a cleanly reconstructed peak at the mass of the Λ is observed. Selecting this band a search is made for cascade particles.

scheme is shown in Fig. 11. The velocity β for neutrals is calculated using the interaction time found from the proton track and shows a clear peak at β=1 for photons. The tail at low velocities is due to additional hits in the calorimeter which were not tagged as photons.

This sample of $p\gamma\gamma\gamma\gamma$ was reconstructed without any knowledge of the scattered electron. The events were selected by missing energy which was lost down the beampipe (Fig. 12) which reduced the combinatorial background by a factor of 2. Four photons were reconstructed in the calorimeter and show peaks for π^0's and η's in Fig. 13. The timing of the photons is consistent with the vertex time derived from the proton in the event and indicates that the timing at the vertex can be determined in the absence of the scattered electron. While we have made tighter cuts for this test case than is practical for the actual data run, we also note that the algorithms are a first and successful attempt to reconstruct these "untagged" data.

6.2 Multiple charged track events

In the case of multiple charged track events, vertex times are computed assuming all possible mass assignments for each track. The vertex time for a given track is then

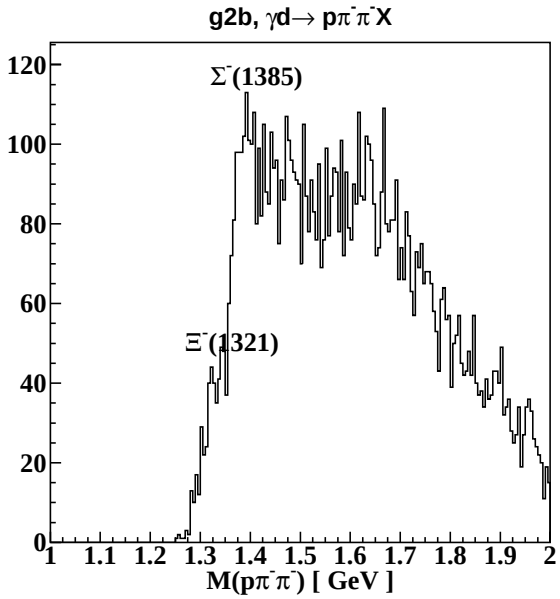

Figure 16: After selecting the bands of Λ's in the previous plot, the $p\pi^-\pi^-$ invariant mass is plotted for all particles.

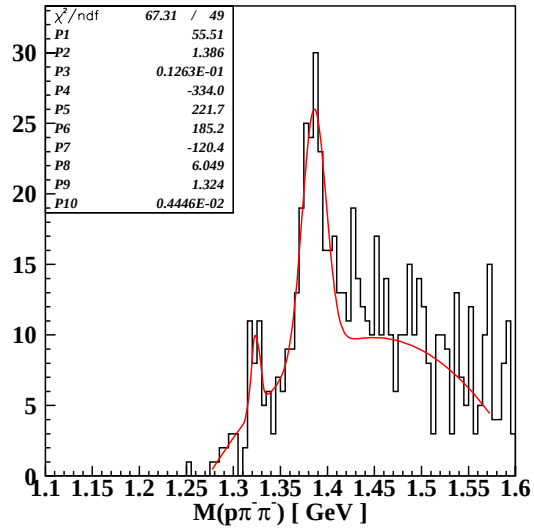

Figure 17: Same as Fig. 16, with the requirement that a K^+ is also detected which tags strangeness production. This additional requirement enhances the $\Sigma^-(1385)$ and the $\Xi^-(1321)$ relative to the background.

selected using the mass assignment that results in the smallest time difference to other tracks. The interaction time for the event is calculated as an average of vertex times for all tracks. In Fig. 14 we show the difference of the vertex times for two hit based tracks from the recent "g2b" run taken in the spring of this year. It shows that this method works very well, and with hit-based track reconstruction the time difference can be defined to better than 1 ns, which provides a very good starting point for time-based tracking.

The reconstruction of multiple tracks in event topologies similar to the present experiment is also demonstrated for the g2b data. Events were selected which contained two π^-'s and a proton. The two possible π^-p combinations were formed and plotted against one another as shown in Fig. 15. Clear bands corresponding to the Λ mass are obtained. By further selecting the band of Λ's, one can plot the invariant mass of the $p\pi^-\pi^-$ which should contain peaks corresponding to the ground state cascade $\Xi^-(1321)$. A shoulder can be seen in Fig. 16. If a K^+ is also required in the event sample as a tag, the peaks are enhanced as shown in Fig. 17 where one can pick out the $\Xi^-(1321)$ ground state and the $\Sigma^-(1385)$ excited state. These plots

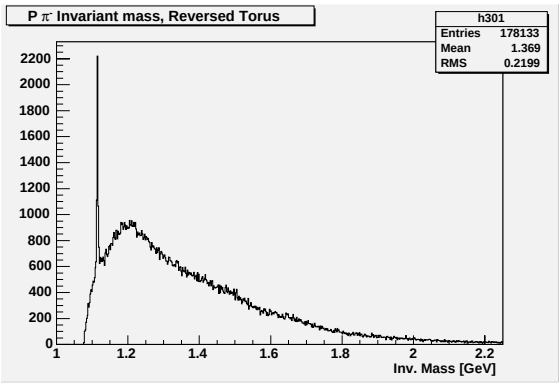

Figure 18: Reconstructed Λs from their $p\pi^-$ decay products with the magnetic field bending negatives away from the axis enhancing the acceptance.

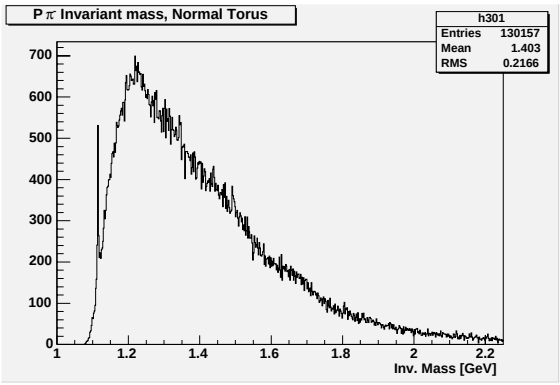

Figure 19: Reconstructed Λs from their $p\pi^-$ decay products with the magnetic field bending negatives into the axis causing a loss of acceptance.

give an indication of resolution and backgrounds without detecting detached vertices. From these plots one can also obtain an acceptance-weighted ratio of the number of $\Xi^-(1321)$ (6) relative to the the $\Sigma^-(1385)$ (56), or approximately 10%.

7 Reconstruction of untagged virtual photon data

In this section we use the sample of e6 data to show that the reconstruction of detached vertices is an effective way of selecting the signal of interest. The e6 experiment took data under several conditions, including both magnet polarities. In Figs. 18 and 19 we show the effect of the magnetic field on the accepted Λs. The acceptance is clearly helped by the reverse polarity of the field which is chosen for this experiment which requires the reconstruction of not one but three negative pions.

The data period with reversed field ran with very similar conditions to those of this proposal (deuterium target, 5.7 GeV beam, outbending negatives and torus field set to 2250 A) and consists of approximately two days of operation. The data were acquired by using the standard electron trigger. At high energies approximately 80% of the data is triggered by hadrons, which are either energetic enough to fire the Cerenkov counter and deposit sufficient energy in the calorimeter, or are produced in combination with other tracks which produce enough energy to satisfy the trigger. Valid electron triggers were removed from the data in order to enrich our sample with "unbiased" events in an attempt to mimic the production using an untagged beam. We note, however, that the trigger bias cannot be completely removed and, although this selection is as close as possible to the proposed conditions, it is still weighted

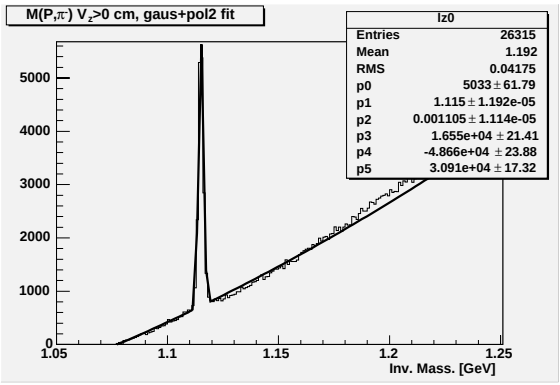

Figure 20: M(p,π^-) invariant mass for all proton π^- combinations for events that have a proton and two π^-. There is no restriction on the location of the reconstructed vertex. The signal-to-background ratio is 3.5 to 1 .

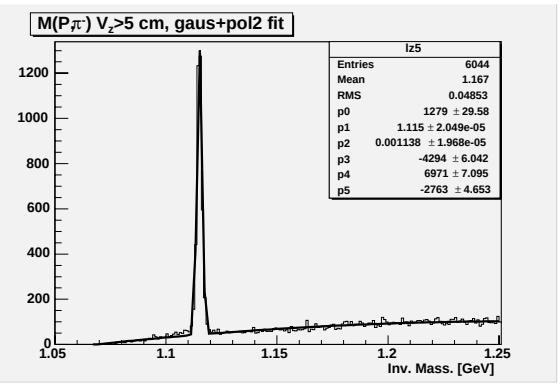

Figure 21: M(p,π^-) invariant mass for all proton π^- combinations for events that have a proton and two π^-. The vertex position is reconstructed downstream of the target ($v_z > 5$ cm). The signal-to-background ratio is 9 to 1.

toward a sample with high energy pions.

The highest momentum negative track is used to estimate the event start time by assuming that it has β=1. For events that have an electron this procedure is of course valid, but only an approximation for the selected sample. For the present analysis, this procedure was not modified, but the routine particle identification required special checks. For example, the predicted vertex times of all particles were required to be the same. Actual analysis of the data would use an iterative procedure to obtain the start time. Nevertheless, we believe that the event selection of events containing one proton and two π^- is relatively clean. The predicted vertex times are shown in Fig. 22 relative to the estimated event start time. The tracks reconstructed to the incorrect beam bucket indicates that the procedure fails about 10% of the time.

7.1 Reconstruction of detached vertices

We use the sample of events which contain one proton and at least two π^-. The goal was to use this sample to select the ground state Ξ^- via the decay chain $\Xi^- \to \Lambda\pi^-$ and $\Lambda \to p\pi^-$, which constitutes the sequence of weak decays in Fig. 4. Due to limited statistics, knowledge of the primary vertex is missing except in a very small subsample of events that contains additional tracks. The invariant mass combinations of the M(p,π^-) is shown in Fig. 20. The signal-to-background is 3.5 to 1.

The pion with the closest M(p,π^-) match to the Λ mass is selected as the daughter particle. The distance of closest approach of the proton track to this pion (< 2 cm)

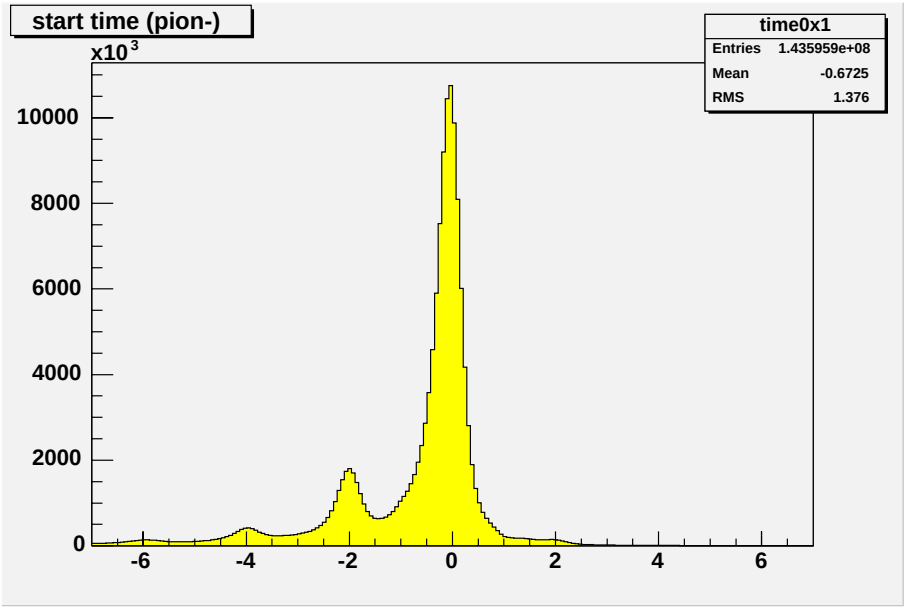

Figure 22: Vertex time for pions relative to the inferred event start time. The side peaks give an estimate of the amount of particle misidentification. The 2 nanosecond peak spacing corresponds to the linac RF frequency.

is used to additionally select the possible $p\pi^-$ tracks which come from Λ decays. The mid-point between the two tracks is chosen to be the Λ decay vertex. The z-component of this vertex is plotted as a function of M(p,π^-) in Fig. 23. The plot shows very clearly that combinations downstream of the target come primarily from true Λ decays. The target extends to approximately 2.5 cm, with a foil located at 4 cm. Fig. 21 shows that by requiring that the vertex be reconstructed outside the target, the background under the Λ peak is substantially reduced. For this sample, the signal-to-background ratio is 9 to 1.

The data reduction as one requires more pions in the event is shown in Fig. 24. Starting with 245M triggers, we have 17M events with one π^-, 0.9M with two π^- and 17k with three π^-. If one additionally requires that the events have valid Λ and Ξ mass combinations, the total event sample is 59 events. This data reduction does not make use of any vertex cuts, only invariant mass reconstruction. Considered all as background events to our signal, we would expect approximately 30 background events per day with the required event topology.

The unpaired, or bachelor, pion can be combined with the Λ candidates to determine the M(Λ,π^-) invariant mass spectrum. The spectrum (not shown) clearly shows the broad peak of the $\Sigma(1385)^-$ strong decay to $\Lambda\pi$, but the ground state $\Xi(1321)^-$

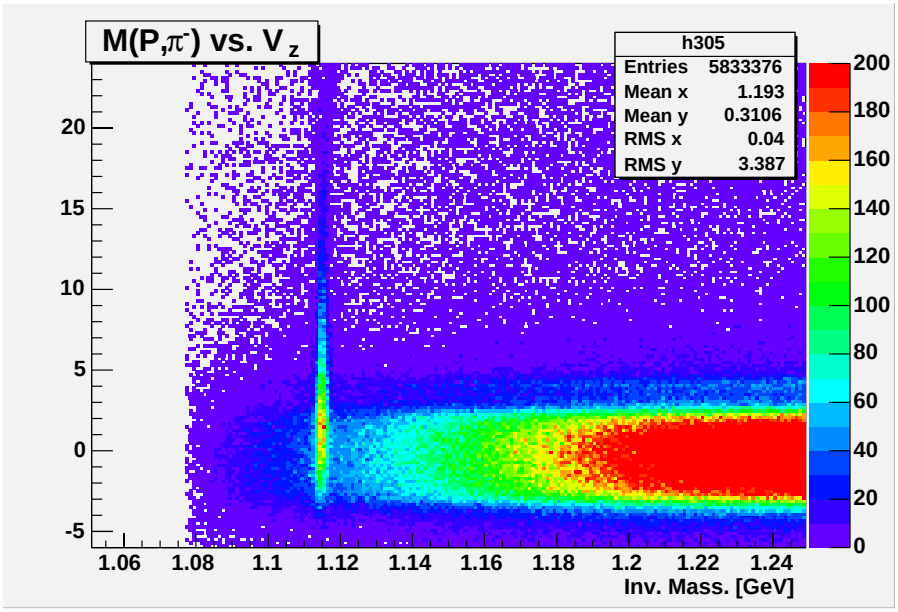

Figure 23: Z position of reconstructed vertex vs the M(p,π^-) invariant mass. The Λ peak shows up clearly for decays inside of the target as well as for decays beyond the target window (Z > 2.5 cm).

peak is not statistically significant. This may be partially due to the trigger bias of this data sample.

8 Acceptance and Monte Carlo simulations

Monte Carlo events were thrown using the phase space event generator GENBOD [16]. The events were generated at a beam energy of 5.7 GeV, outbending magnetic field at 2250 A, assuming a $1/E_\gamma$ dependence for the bremsstrahlung spectrum and modulated assuming a t-dependence of the form:

$$\sigma \sim \exp(-2t), \tag{13}$$

where t is the four momentum transfer to the two kaons. These were used to compute the acceptance for the following decays:

1. $\Xi_5^{--} \rightarrow \pi^-\pi^-\pi^- p$
2. $\Xi_5^{+} \rightarrow \pi^+\pi^-\pi^+ n$

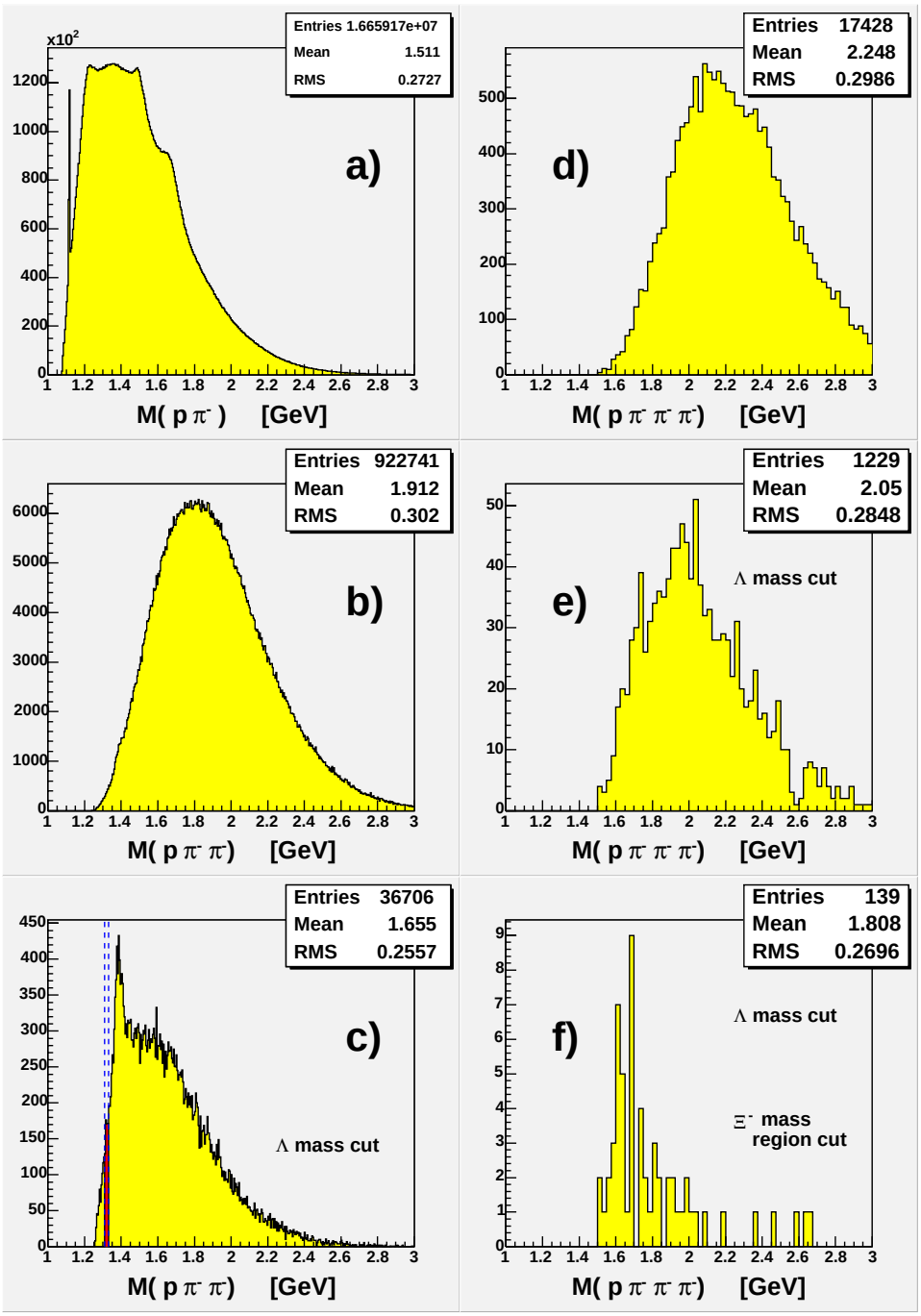

Figure 24: Event rate reduction as one requires more pions in the event and when one requires that these reconstruct to either a Λ or Ξ mass. The plots on the left show the M(p,π^-) mass (a), the M(p,π^-,π^-) (b) the M(p,π^-,π^-) when a valid Λ is found (c), and the M(p,π^-,π^-,π^-) invariant mass for all events (d), requiring a Λ (e) and, a M(Λ,π^-) mass between 1.31 and 1.33 GeV (Ξ mass region indicated in c) (f).

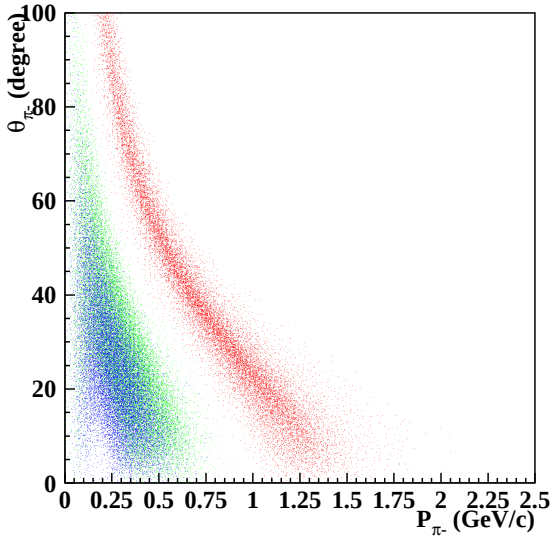

Figure 25: Angle vs. momentum distributions for Monte Carlo generated π^- from the decay sequence $\Xi_5^{--} \rightarrow \pi^-\pi^-\pi^- p$. The red band comes from the decay $\Xi_5^{--} \rightarrow \pi^-\Xi^-$, the green band from the $\Xi^- \rightarrow \pi^-\Lambda$, and the blue band from $\Lambda \rightarrow \pi^- p$.

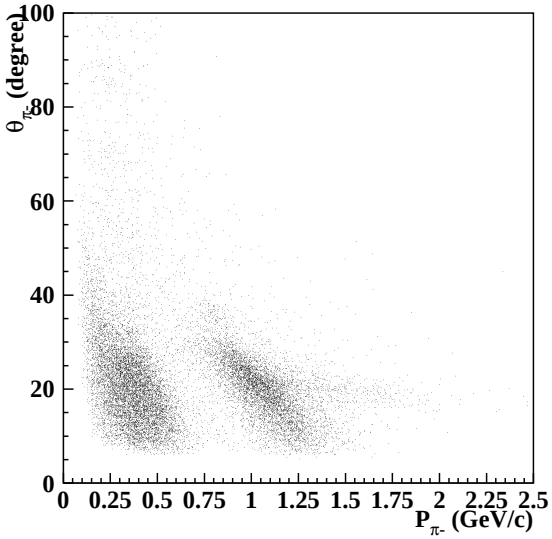

Figure 26: Angle vs. momentum distributions for the reconstructed π^- from the Monte Carlo generated decay sequence $\Xi_5^{--} \rightarrow \pi^-\pi^-\pi^- p$.

3. $\Xi_5^+ \rightarrow \pi^+\pi^0\pi^- p$

The generated angle and momentum distributions for pions in reaction 1) are shown in Fig. 25. After a full GSIM (GEANT Monte Carlo for CLAS) simulation of the events, the distributions of the reconstructed pions are shown in Fig. 26. The low momentum pions at large angles are lost as well as pions at angles less than 8 degrees. Several acceptance scenarios were computed. For the case where we require tracks in three sectors, which we might need to impose at the trigger level, the acceptance for this channel is 0.15%. The loss of events compared to a 2-sector trigger is shown in Fig. 27 and is only about 20%. However, the reduction in trigger rate for the 3-sector requirement is considerable.

The acceptance for the decays of the $\Xi_5^+ \rightarrow \pi^+\pi^-\pi^+ n$ is quite small ($\sim 0.02\%$) so this decay will be very difficult to detect. The decay $\Xi_5^+ \rightarrow \pi^+\pi^0\pi^- p$ is computed to be 2.5 times smaller. The π^0 signal may have less background than the neutron, but in any case the expected detection rate for either channel is very small.

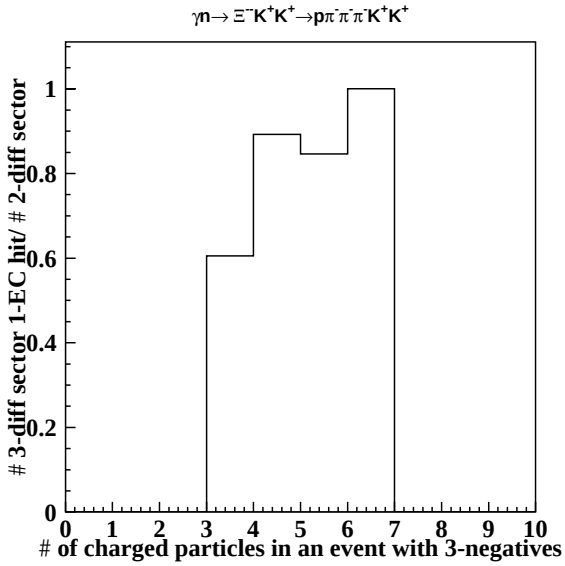

Figure 27: Fraction of reconstructed Ξ_5^{--} events that have hits in three sectors and minimum energy deposition in the calorimeter compared to events that have hits in at least two sectors.

9 Backgrounds

The reconstruction of the decay sequence of the exotic cascades to narrow states via detached vertices will provide a very clean signature. Nevertheless, there will be backgrounds which will mimic the signal and need to be understood in order to determine our experimental sensitivity. The backgrounds will include both physics related backgrounds and accidental reconstruction of unrelated tracks.

The physics backgrounds will include the production and decay of excited cascades. In this case the decay sequence will be identical to the one depicted in Fig. 4. However, a π^- from the primary vertex will not form a narrow mass peak when combined with the measured ground state Ξ^-. This background will be proportional to the inclusive rate of excited cascades. Taking the cross section to be approximately 100 nb, we expect this background to be comparable to the size of our signal.

The accidental reconstruction of unrelated tracks will include a combination of real production of weakly decaying particles, such as Λs, in combination with pions which decay inside the Region 1 drift chambers and appear to be coming from a second detached vertex. During low intensity photon running, but without making use of vertex reconstruction, we see very low background rates which are consistent with

accidental coincidences. The fraction of events under the ground-state $\Xi^-(1321)$ is less than 10%, but is closer to 100% for the $\Xi^-(1530)$. We expect that the reconstruction of detached vertices will provide a significantly cleaner signature.

Based on the total number of events in the e6 data sample with one proton and three negative pions which have valid Λ and Ξ mass combinations, described in Section 7.1, we estimate a total of 600 background events during a 20 day run. This estimate is conservative as it ignores any benefit from vertex reconstruction.

10 Figure of merit

The relative merits of various methods of producing and detecting the pentaquark cascade particles Ξ_5 are tabulated in Table 4. Many entries in this table are estimates, but are collected to give a global picture of the benefits of each measurement. The factors in each column are arbitrarily normalized but are proportional to the number of expected events in the final data sample, except of the signal/background ratio which is intended to provide guidance to the ease of extraction of the signal. We compute a figure-of-merit (FOM) based on the product of all factors in the table. Based on this FOM we conclude that the maximum sensitivity is obtained using an untagged beam of virtual photons at a luminosity of $10^{34}\mathrm{cm}^{-2}\mathrm{s}^{-1}$. The same rate could be obtained with an untagged beam of real photons with either a thicker target and/or increasing the maximum power limit on the tagger dump.

Table 4: Estimates of various factors that contribute to the production, detection and reconstruction of cascade particles. The FOM is estimated as the product of all factors. For the case of a hydrogen target using missing mass, we assume that approximately 50% of the K^+'s decay and are not reconstructed. For the untagged running on deuterium we use the sum of the contributions from the proton and neutron.

Run Conditions	Channel	σ (nb)	Thresh	Branch	Flux	Signal/ Back	Acc	FOM
Tagged γ hydrogen Miss mass real γ	Ξ_5^{--}	1	0.7	~ 0.25	0.3	$0.1 \times$ 0.3/Flux	$\sim$3%	0.02
	Ξ_5^{-}	10	1.0	~ 0.25	0.3	$0.1 \times$ 0.3/Flux	$\sim$10%	0.8
	Ξ_5^{0}	5	1.0	~ 0.08	0.3	$0.1 \times$ 0.3/Flux	$\sim$1%	0.01
	Ξ_5^{+}	1	1.0	~ 0.11	0.3	$0.1 \times$ 0.3/Flux	<0.1%	0.0003
Untagged deuterium real γ	Ξ_5^{--}	11	1.0	0.32	>0.3 $\times$ tgt/18	~ 0.5	0.15%	0.08
	Ξ_5^{-}	15	1.0	0.38	>0.3 $\times$ tgt/18	~ 0.5	$\sim$0.06%	0.05
	Ξ_5^{0}	6	1.0	0.11	>0.3 $\times$ tgt/18	~ 0.5	$\sim$0.05%	0.005
	Ξ_5^{+}	1	1.0	0.09	>0.3 $\times$ tgt/18	~ 0.5	$\sim$0.02%	0.0003
Untagged deuterium virtual γ	Ξ_5^{--}	11	1.0	0.32	L/L_0	~ 0.5	0.15%	0.26
	Ξ_5^{-}	15	1.0	0.38	L/L_0	~ 0.5	$\sim$0.06%	0.17
	Ξ_5^{0}	6	1.0	0.11	L/L_0	~ 0.5	$\sim$0.05%	0.02
	Ξ_5^{+}	1	1.0	0.09	L/L_0	~ 0.5	$\sim$0.02%	0.0009

11 Summary

We propose to measure the production of pentaquark Ξ_5 cascade particles with an untagged virtual photon beam to achieve the highest possible luminosity with CLAS. The cascade states will be detected by reconstructing their decay products to take advantage of the detached vertices of the weakly decaying secondary particles.

The nominal conditions for this run are as follows:

- Electron beam energy = 5.7 GeV.
- Deuterium target 0.5 cm in length
- 20 days of operation
- Torus magnet set to negative polarity to bend negative particles away from the axis.

The significance for detecting the Ξ_5^{--} is given roughly by $S/\sqrt{(B)}$. We estimate the total yield, S, to be 460 counts, with estimates for the Ξ_5^- (Ξ_5^0) to be about two (ten) times smaller. The significance, N_σ, expressed in terms of the number of "σ" can be expressed more generally as

$$N_\sigma(\Xi_5^{--}) \;=\; \frac{\sigma \times BR}{0.16\,nb}\sqrt{\frac{R}{20\,days}}\sqrt{\frac{B(estimate)}{B}} \qquad (14)$$

where $\sigma \times BR$ is the actual cross section times branching ratio of the Ξ_5 pentaquark, R is the running time of the experiment, $B(estimate)$ is our estimate of 600 events under the signal peak for 20 days of running, and B is the actual number of background events under the Ξ_5 peak. This expression allows one to estimate the significance of the proposed measurement for other conditions than those assumed in this proposal.

With our estimate for the background of 600 counts, we estimate a significance for the Ξ_5^{--} of 21"σ".

A Methods of producing an untagged photon beam

There are two options for producing an untagged photon beam. The first involves the use of the tagging magnet and radiator in a way similar to that used for tagged photon beams, but ignoring the information in the tagging spectrometer because the high accidental coincident rate makes this data almost useless. We will refer to this option as the "untagged photon beam option." The second method, which we will call the "untagged electron beam option," involves sending the electron beam through the target and using the high virtual photon flux produced at very low Q^2. Again there are various considerations that might lead to the choice of one method over the other. The issues are given below:

Limitations to the maximum possible flux The untagged electron beam option is limited by the performance of the drift chambers to a luminosity of $10^{34} cm^{-1} s^{-1}$. The untagged photon beam option is limited on the one hand by the power limits on the photon beam dump (800 W, or 140 nA for a 5.7 GeV beam), and by the thickness of the radiator which contributes to the size of the beam when it becomes thicker than 10^{-3} radiation lengths where the multiple scattering angle of the electron in the radiator is equal to the critical angle.

Transverse size of the beam The electron beam can be used to determine the interaction in the target to an accuracy of less than 0.2 mm (transverse dimension), and has the additional advantage that monitoring and control of the beam is simplified during the experiment. The natural size of the untagged photon beam is determined by the critical angle ($m_e/E = 9 \times 10^{-5}$ rad at 5.7 GeV) or a half width of 2 mm at the position of the CLAS target. Although we do not expect to require higher fluxes, for rates above $2 \times 10^8 \gamma/s$ between 4 to 5.5 GeV, multiple scattering in the radiator will begin to contribute significantly to the size of the photon beam.

Production of backgrounds in the target The electron beam produces a large number of Møller electrons in the target which produce hits in the entire detector. This background limits the rate at which electron-beam experiments can take data. While we do not expect this to be the direct limit to the maximum luminosity, the number of hits in the detector increases the size of the event which ultimately has an impact on the maximum rate of triggers which can be handled by the DAQ system. The DAQ rate will limit the maximum luminosity we can take.

By contrast, (tagged) photon beam experiments have relatively few background hits and track segments which are unrelated to the hadronic interactions of

interest. However, we do not have experience operating CLAS in the presence of photon beams of the intensities which are proposed here. But we still expect that due to the absence of direct Møller production in the target, that the CLAS detector should be substantially less active than in the case of the untagged electron beam option. A quantitative evaluation of the benefits of the smaller background rate will take some time and has not been completed yet.

After evaluating the benefits and limitations of the each of the options available, we conclude that the best option is to use the untagged electron beam method incident on a 0.5-cm deuterium target.

A.1 Maximum tagged photon flux

For reference we give the estimated rate for hadronic production in g6c, which ran at the highest luminosity of tagged photon experiments to date.

$$F_\gamma = \frac{I_e}{e}\,\mathrm{rad}\int_{kmin}^{kmax}\frac{g(w)}{k}dk \tag{15}$$

$$g(w) = \left[1+(1-w)^2-\frac{2}{3}(1-w)\right]+\frac{(1-w)}{9\ln(183/Z^{\frac{1}{3}})} \tag{16}$$

$$w = \frac{k}{E} \tag{17}$$

$$F_\gamma \approx \frac{I_e}{e}\,\mathrm{rad}\,\ln(\frac{kmax}{kmin}), \tag{18}$$

where I_e is the electron beam current, rad is the thickness of the radiator in units of radiation length, k is the energy of the photon, $kmin$ and $kmax$ are the limits of the tagging range, and Z is the atomic number of the radiator. The last equation is the standard $1/\mathrm{E}_\gamma$ approximation to the photon flux and is easily integrated to give rate estimates. However, it does underestimate the hadronic rates especially at low photon energies by approximately 20-30%. For g6c which ran at the highest photon (tagged) photon flux to date, we have the following parameters

$$I_e = 40\,nA \tag{19}$$

$$t = 1.26 g/cm^2 \tag{20}$$

$$\mathrm{rad} = 3\times 10^{-4} \tag{21}$$

$$\mathrm{kmin} = 4.8\,GeV \tag{22}$$

$$\mathrm{kmax} = 5.2\,GeV \tag{23}$$

$$F_\gamma \approx 6\,MHz \tag{24}$$

$$
\begin{aligned}
Rate_{tot}(Hz) &= 52\,KHz && (25)\\
\sigma_{\Xi} &= 10\,nb, && (26)\\
Br(\Xi_5^{--} \to \pi^-\pi^-\pi^- p) &= 0.32 && (27)\\
Acc &= 1.5 \times 10^{-3} && (28)\\
N_{\Xi}(20\,days) &= 150 && (29)
\end{aligned}
$$

The number of cascades produced in a 20 day run is estimated using the flux between 4 and 5.5 GeV, which increases the photon flux from 6 to 24 MHz. The rates using an untagged photon beam can be calculated by scaling the previous numbers by the following factors:

$$
Rate = Rate_{g6c} \times \frac{\mathrm{rad}}{3 \times 10^{-4}} \times \frac{\mathrm{L_{tgt}}}{18\mathrm{cm}} \times \frac{I_e}{40nA} \qquad (30)
$$

In order to produce the same number of cascades as produced using the virtual photon flux (460 cascades) and a 0.5 cm deuterium target, we need to increase the photon flux by a factor of of $(460/150)\times(18/0.5) = 110$. For the nominal tagger dump rating of 800 W, the current can be increased by a factor of 140/40, so the radiator thickness would need to 10^{-2} radiation lengths. This is ten times the limit required to keep multiple scattering from dominating the beam spot size. We note, however, that by cooling the tagger dump, the current limit can be increased by an order of magnitude.

B CLAS DAQ performance

We review the current status and planned upgrades to the system. In describing the CLAS DAQ performance, it is convenient to consider the DAQ system as a 2-step process. The first step is data conversion in ADCs and TDCs or data rejection by the Level-2 trigger. The second step is data collection: from ADC and TDC readout up to writing the data file.

B.1 ADCs/TDCs conversion, Level-2 rejection, and dead time

Under normal conditions the CLAS DAQ dead time is defined by the conversion time in the ADCs and TDCs. Normal conditions means there are no significant delays in other DAQ components such as readout lists, etc.

Current status. CLAS DAQ has three types of boards which contribute to the dead time, although it is defined by the slowest one which is the FASTBUS LeCroy 1872 TDC. That board has a conversion time of 10μs + 2.5μs/hit. Usually we have about 35-40μs for electron runs and 50μs for photon runs (in the last case we are

using one 16-pair connector per TDC board for tagger T-counters, and all 16 signals are usually present).

Taking into account 40μs as a typical conversion time we can expect 4% dead time at 1kHz event rate, 8% at 2 kHz, 12% at 3 kHz and so on, although real dead time value may be slightly bigger (for example 14% instead of 12% at 3kHz) for reasons we have not investigated yet.

This does not necessarily imply that the conversion time will be 40% at 10kHz. The current limit for electron runs at high energy is somewhere around 3kHz. It is defined by other DAQ components and will be discussed below. It should be also mentioned that changing trigger conditions may change the dead time dramatically as every extra hit in a TDC will increase the conversion time by 2.5μs.

The Level-2 trigger may speed up the DAQ system significantly due to its ability to the stop conversion process before it finished and discard the entire event. It takes 7μs which is much smaller than the 35-40μs conversion time. Unfortunately, the CLAS Level-2 logic is very sensitive to the noise in Drift Chamber. Being quite efficient for 1-2GeV beam, it became almost useless above 5GeV. On the other side we never tried a 3-sector coincidence which can be more efficient.

Possible improvements. We have a plan to replace the LeCroy 1872 TDCs by the summer of 2004. New boards will be deadtimeless, so the CLAS DAQ dead time will be defined by the FASTBUS LeCroy 1881 ADCs conversion time which is 12μs fixed. It should decrease the CLAS DAQ dead time by a factor of 2.5, and make it insensitive to the number of hits. That plan requires considerable effort, but if completed we should be able to go up to 10kHz with a 15% dead time, if all other CLAS DAQ components can handle such rate.

B.2 Data collection

The whole data collection process starting from ADC/TDC readout can be considered as a chain of pipe-line components. We can estimate the performance of every component separately from others, as long as they do not share the same resources (CPUs, memory etc). Otherwise we have to consider them together as one group. The final DAQ system performance will be defined by the slowest component.

The first group of components includes 3 programs running in the Readout Controller board (ROC): first readout list (ROL1) called by hardware interrupt, second readout list (ROL2) running in pooling mode and networking task (NET) running as separate VxWorks job. All three programs share the same CPU and the same memory. The largest contribution to the deadtime comes from the Drift Chamber ROCs because of the large amount of hits that need to be processed. For electron runs it takes typically 80-120μs for ROL1, 80-100μs for ROL2 and unmeasured (yet) time for NET. Together with system overhead we need more then 300μs per event

which sets a 3kHz event rate limit.

The second group of components which run on the SMP are the Event Builder (EB), Event Transfer system (ET), the Level3 trigger (L3) and the Event Recorder (ER). At the present time we can run up to 18MB/s without experiencing any delays.

Possible improvements. ROC: a multiprocessor system will be used. This project has begun but with reduced priority, and most of the work would be done by the CODA group. If allocated sufficient priority, it could be finished by summer of 2004. Running ROL1, ROL2 and NET on separate processors we can probably reach event a rate about 7-8 kHz.

SMP: EB and ER are the two components which set out current DAQ limit. Our file system was upgraded recently to VERITAS which pushed our writing speed from about 22MB/s to the 35MB/s. The Event Building part of EB was redesigned as multi-threaded, and should not set a limit as soon as we have 8 CPUs. The present limitation is the input part of EB, namely reading data from network sockets. To avoid a bottleneck at that place, several network cards must be used, as was done already for the tagger FASTBUS crate. Of course, buying a new SMP will also improve that part of the DAQ dramatically. SUN now provides a computer with CPUs which are twice as fast as our present computer, and more processors. Although a new SMP is quite expensive it is a fast solution if we want to speed up that part of CLAS DAQ without extra efforts from our side.

B.3 DAQ summary

We can summarize this discussion with the following points:

1. It seems impossible to speed up the CLAS DAQ system without upgrades.
2. LeCroy 1872 TDCs replacement will decrease conversion time to 12μs and eliminate dependence on hit multiplicity.
3. Using a multiprocessor system in the ROCs will extend the back-end limit up to approximately 7-8 KHz.
4. We can increase the data rate by an additional factor of 1.5 with our current SMP, but to go further we need to buy a new one.

References

[1] T. Nakano *et al.*, (The LEPS Collaboration) Phys. Rev. Lett. **91**, 012002 (2003) [arXiv:hep-ex/0301020]

[2] V.V. Barmin *et al.*, (The DIANA Collaboration), Phys. At. Nucl., **66**, 1715 (2003) [arXiv:hep-ex/0304040]

[3] S. Stepanyan *et al.*, (The CLAS Collaboration) to be published in Phys. Rev. Lett. (2003) [arXiv:hep-ex/0307018]

[4] J. Barth *et al.*, (The SAPHIR Collaboration) Phys. Lett. **B572**, 127 (2003) [arXiv:hep-ex/0307083]

[5] A.E. Asratyan *et al.*, to be published in Phys. Atom. Nuclei (2004) [arXiv:hep-ex/0309042]

[6] W. Lorenzon, HERMES Collaboration, contribution to the Penta-Quark 2003 Workshop, JLab, Nov 6-8, 2003.

[7] Updates to all work can be found in the presentations to the Penta-Quark 2003 Workshop, JLab, Nov 6-8, 2003,

`http://www.jlab.org/intralab/calendar/archive03/pentaquark/program.html`.

For a review of the phenomenology and models, see B. Jennings and K. Maltman, hep-ph/0308286

[8] D. Diakonov, V. Petrov, and M. Polyakov, Z. Phys. A **359**, 305 (1997).

[9] D. Diakonov and V. Petrov *et al.*, arXiv:hep-ph/0310212

[10] C. Alt *et al.*, (The NA49 Collaboration), arXiv:hep-ex/0310014

[11] J. Pochodzalla (The WA89 Collaboration), contribution to VIII International Conference on Hypernuclear and Strange Particle Physics, Jefferson Lab, October 14-18, 2003

`http://www.jlab.org/intralab/calendar/archive03/HYP/talks/Pochodzalla,%20J.pdf`

[12] W. Liu, contribution to the Penta-Quark 2003 Workshop, JLab, Nov 6-8, 2003.

[13] B.A. Mecking *et al.*, Nucl. Instr. and Meth. **503**, 513 (2003)

[14] Y.Oh, H. Kim and S.H. Lee, arXiv:hep-ph/0310117

[15] C.E. Carlson *et al.*, arXiv:hep-ph/0310038

[16] The CERN Program Library, W515,

`http://wwwasd.web.cern.ch/wwwasd`